Journal of Thermal Analysis, Vol. 54 (1998) 825-835

ANALYSIS OF PRECIPITATION HARDENING OF 6061/10% SiC COMPOSITE BY DIFFERENTIAL SCANNING CALORIMETRY

L. Lu, M. Gupta and M. O. Lai

Department of Mechanical and Production Engineering, National University of Singapore
Singapore 119260

(Received March 24, 1997; in revised form January 8, 1998)

Abstract

The precipitation of a supersaturated 6061 Al alloy reinforced with 10% SiC_p was monitored by using a DSC technique. DSC thermal curves were used to predict peak-aging temperatures and durations. The activation energies for precipitation of the β″ phase were found to increase with elevation of the solution temperature from 510 to 600°C, and hence the peak-aging temperature and duration also increased. Microstructural examination revealed an increase in grain size when a high solution temperature was applied. To compare predicted peak-aging temperatures and durations, hardness measurements were carried out after artificial aging. The studies revealed that peak-aging hardening was obtained when the aging temperatures and durations corresponded to about 95% to 97% precipitation of β″ phase from conversion plots.

Keywords: Al alloy, DSC, hardness measurement, peak-aging, precipitation

Introduction

Differential scanning calorimetry (DSC) is a useful technique for the monitoring of complex changes in the microstructural and physical features of materials. A differential scanning calorimeter measures the temperatures and heat flows associated with transitions in materials. Such measurements provide quantitative and qualitative information about the physical and chemical changes involved in endothermic or exothermic processes. For some such transitions, DSC measurements can reveal not only the temperatures at which the transitions occur and how much total heat is associated with each transition, but also valuable information on the kinetics of reaction. One of the uses of DSC is for measurement of the extent of phase transformations.

1418–2874/98/ $ 5.00

Akadémiai Kiadó, Budapest
Kluwer Academic Publishers, Dordrecht

Because of the high sensitivity of DSC, it was earlier used together with transmission electron microscopy (TEM) to measure precipitation in 7000 series Al alloys [1, 2]. Endothermic and/or exothermic reactions were observed within the wide temperature range from 20 to 500°C. A DSC study of fatigue-induced microstructural changes in 7050 Al alloy has also been carried out [3]. However, DSC does not detect changes in the bulk precipitate after fatigue cycling in the elastic strain range, while fatigue cycling with non-zero plastic deformation causes significant modification to the thermal curve during the dissolution of Guinier-Preston (GP) zones. Different rates of cooling of solution-treated Al alloys can also influence DSC thermal curves [4]. Such curves demonstrate that the air-cooling of specimens (2124 Al alloy) from 496°C to either 454, 399 or 343°C prior to the final water quenching leads to a slight increase in the S' precipitate peak temperature. However, the latter temperature is dramatically elevated by interrupted quenching. DSC analyses and mechanical tests have shown that ceramic reinforcement generally enhances the rate of aging of composites with respect to the unreinforced metal matrix, but it does not affect the aging sequences [5–7]. This behaviour can be attributed to higher dislocation densities in the composites, induced by the difference in the coefficients of thermal expansion of the ceramic and matrix metal. Dislocations are known to be possible sites for heterogeneous nucleation [8]. In other cases, aging effects in MMCs can be accelerated by the generation of an elastic residual stress field [9]. Papazian *et al.* [3] reported that the precipitation sequence was not affected by SiC_p reinforcement in a 2124 Al alloy, but that the volume fraction of GP zones decreased with increase of the amount of SiC_p. Hence, it was suggested that the decrease in the volume fraction of GP zones was due to a SiC_p-induced increase in quench sensitivity [11]. However, this sensitivity was not observed in the SiC whisker-reinforced MMCs [11]. TEM revealed no precipitates in SiC whisker-reinforced MMCs in the solution-treated and quenched state. The peak-aging time for whisker-reinforced Al–Cu MMC was significantly retarded. This result seems to contradict data from other measurements [3]. Another TEM study showed a typical dislocation density of $3.1 \cdot 10^{10}$ m^{-2} for the solutionized and as-quenched alloy. The dislocation density in the 10 vol.% Al_2O_3 MMC was found to be $4.5 \cdot 10^{12}$ m^{-2}, while that for the 15 vol.% Al_2O_3 MMC was $7.3 \cdot 10^{12}$ m^{-2} [12].

The present study focuses on the influence of the solution temperature of a 6061/10 wt.% SiC_p composite on the kinetics of precipitation of the β'' phase. DSC thermal curves were utilized to calculate the activation energies after different heat treatments. Precipitation conversion curves were constructed and micro and macro hardnesses were measured for the prediction of aging temperatures and durations [13].

Experimental

Conventionally cast 6061 (Al–1.0 wt.%, Mg–0.6 wt.%, Si–0.2 wt.%, Cr–0.27 wt.% Cu)/10 wt.% SiC_p extruded to 10 mm diameter, was sectioned into pieces 15 mm in length with a wire-cutting machine (for a detailed process procedure, refer to [13]). Cut specimens were solution heat-treated at four different temperatures, 510, 530, 540 and 600°C, for 4 h, followed by water quenching to room temperature. Because of the high cooling rates, the formation of stable Mg_2Si phase was not possible and a supersaturated solid solution was obtained. The heat-treated specimens were then cut into smaller pieces about 0.3 mm thick, using a diamond saw with a very low load, for DSC measurements. A TA 2910 DSC instrument was employed in the present study. The fact that there was no transition for SiC_p in the temperature range of interest suggested that only the effective mass of the MMC sample needed to be taken into account [14]:

$$(\text{sample mass})_{\text{effective}} = (\text{sample mass})_{\text{actual}} - \text{mass of } SiC_p \quad (1)$$

The DSC baseline and temperatures were calibrated using In and Al. Continuous temperature scanning was applied at 2, 5, 10 and 20°C min^{-1}. DSC results were analysed in accordance with the ASTM E698-79 approach [15] and the Kissinger method [16].

To evaluate the relationship between the hardness and the degree of precipitation, the microhardness and the superficial Rockwell hardness were measured. At least five readings of hardness measurement were taken on each specimen. The grain size was measured and analysed by means of a Quantimet 520.

Results and discussion

Figures 1 and 2 show two sets of typical DSC plots for specimens solution-treated at 510 and 600°C, respectively. In the temperature range between room temperature and 350°C, only three exothermic peaks, A, B and C in Figs 1(a) and 1(c), can be seen. Additionally there is a very small exothermic peak, A' in Fig. 1(c), at about 85°C. Clearer evidence can be seen from Figs 2(a) to (d). Three exothermic peaks are visible in Fig. 1(d) and Figs 2(b) and (c). All the exothermic peaks, A, B and C, were observed to shift to higher temperatures, indicating that the rate of formation of the precipitates is strongly influenced by the reaction kinetics. Similar phenomena have been reported by Dutta and Bourell [9].

The precipitation sequence in supersaturated Al–Mg–Si alloys is [18]

$$\text{supersaturated solid solution} \rightarrow \text{GP Zones} \rightarrow \beta'' \rightarrow \beta' \rightarrow \beta$$

The precipitation sequence given above demonstrates that the precipitation of a supersaturated specimen involves three stages of change during heating. In the

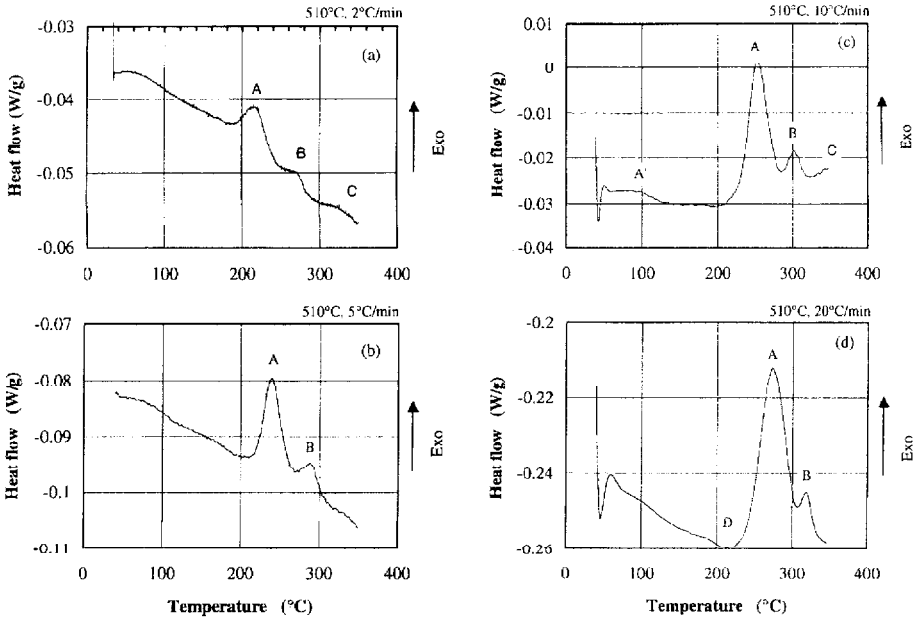

Fig. 1 DSC measurements on specimens solution-treated at 510°C; Heating rate: (a) 2, (b) 5, (c) 10 and (d) 20°C min^{-1}

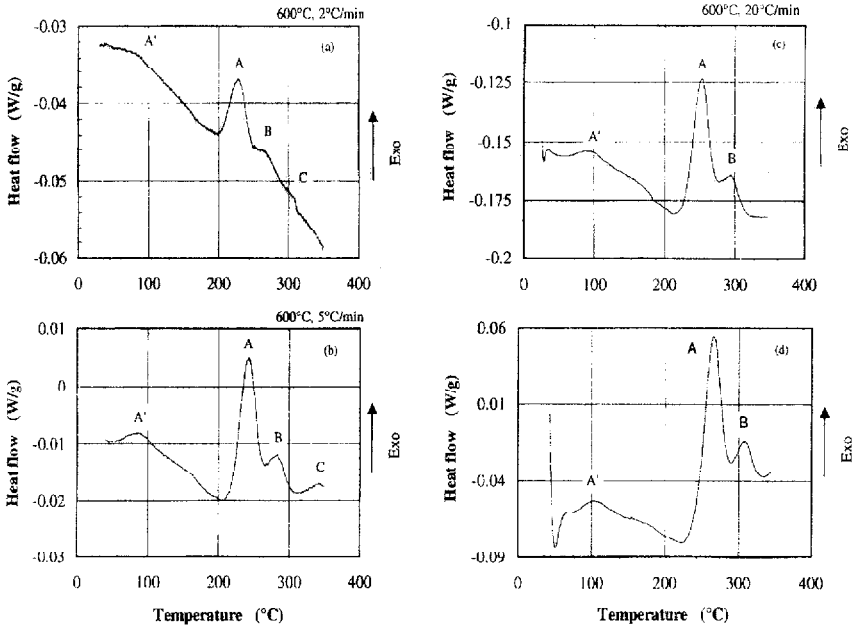

Fig. 2 DSC measurements on specimens solution-treated at 600°C; Heating rate: (a) 2, (b) 5, (c) 10 and (d) 20°C min^{-1}

first stage of aging, very fine, needle-shaped GP zones orientated in the <001> direction of the matrix are formed. The nucleation of the GP zones leads to an initial increase in free energy. The growth of the GP zones leads to a decrease in internal energy, enabling an exothermic reaction to start. Further increases in temperature and aging time cause an apparent three-dimensional growth of the GP zones to rod-shaped particles with a structure corresponding to that of a highly-ordered Mg_2Si phase. The growth of the GP zones to the Mg_2Si phase is accompanied by heat release. In the third stage, the highly-ordered β' phase undergoes transformation to the equilibrium Mg_2Si phase. It is believed that the second exothermic peak, B, is due to the transition from β'' to a hexagonal structure of β'. This transition has been confirmed by means of TEM by several researchers [12, 19, 20]. According to Badini [21], the first exothermic peak, A', in the DSC plot (Fig. 2(b)) is an indication of the formation of GP zones. However, Dutta *et al.* [12] have indicated that peak A' is actually due to the clustering of Si, while peak A is due to the formation of GP zones (and β'') and peak B corresponds to the formation of β'. The last exothermic peak represents the formation of equilibrium β phase. Comparison of the two sets of DSC curves reveals that the heat involved in the clustering of Si is higher in the specimens solution-treated at 600°C than in those solution-treated at 510°C, presumably because of the local melting of the eutectics at 600°C.

For the specimens solution-treated at 510°C, the two exothermic peaks A and B can be clearly separated. However, for the specimens solution-treated at 600°C, the two exothermic peaks are closer to each other, indicating that the β'' to β' transition starts before the β'' phase is fully formed. It can be deduced from this observation that, to obtain maximum precipitation hardening from aging, the solution temperature should be selected so that the two exothermic peaks are separated from each other.

Activation energy for precipitation

The relative rates at which precipitation takes place depend upon the respective diffusion rates in addition to solubilities and alloy content. Determination of the kinetics of a transformation by means of DSC is based on two assumptions: (a) the heat flow relative to the instrument baseline is proportional to the rate of reaction, and (b) the temperature gradients through the sample, and the temperature difference between the sample and the reference, are small.

According to ASTM-698, the kinetics of a transition can be analysed as a function of the changes in peak size and peak temperature as the heating rate is changed. The rate of reaction (precipitation in the present study) can be expressed by the general rate law

$$\frac{dx}{dt} = k(1 - x)^n \tag{2}$$

and

$$k = Z\exp\left(\frac{-E}{RT}\right) \tag{3}$$

where x is the fractional conversion (in the present case, it represents the percentage of precipitates), t is the time (min), n is the reaction order, k is the specific reaction rate constant, Z is the pre-exponential factor, E is the activation energy (J mol^{-1}), R is the gas constant (8.32 J mol^{-1} K^{-1}) and T is the temperature (K). The activation energy can also be calculated by using the Kissinger method [16].

For specimens solution-treated at the four above-mentioned temperatures, the activation energies E and pre-exponential factors Z of peak (refer to Figs 1 and 2) are listed in Table 1. The two results are in good agreement.

The variation in activation energy with solution temperature is plotted in Fig. 3. It can be seen that the activation energy increases with increase of the solution temperature. It was expected that quenching from a higher solution temperature would lead to a greater residual dislocation density around the reinforced particulates. This would make precipitation easier for semi-coherent phase, i.e. a decrease in activation energy. However, an increase in activation energy was found in the present study. The increase in activation energy with increase of the solution temperature can mainly be attributed to three factors: (a) a high dislocation density, (b) grain growth at high solution temperatures, and (c) relaxation of internal energy.

Because of the difference in coefficient of thermal expansion, high dislocation densities are generated during quenching from the solid-solution temperature. The growth of precipitates in the composite is a consequence of heterogeneous nucleation of precipitates along the dislocations. Aging is accelerated for higher dislocation densities. However, Suresh *et al.* [17] reports that, if the density of dislocations is high enough, any further increase in dislocation density is not responsible for the acceleration of aging. Suresh measured the peak aging times for Al alloys reinforced with 6, 10 or 20 vol.% SiC_p, and found that the peak aging times for the three MMCs were similar. Therefore, although quenching from 600°C may generate a high dislocation density, it does not strongly influence the peak-aging time.

Measurement of the grain size showed that the equivalent diameter of grains increased from 77 to 96 μm when the solution temperature was raised from 510 to 600°C. Since the driving force for the transformation from the GP to the β′ phase is the high strain field, the energy cost for accommodating the strain field is lower if a high density of dislocations is present. A high dislocation density makes precipitation easier when a balancing between the stress fields due to dislocations and phase nucleation occurs. Since grain boundaries are locations of higher disorder and energy than those areas far from the grain boundaries, this suggests that the existence of a higher strain field within the fine-grained MMC

means that these are preferred sites for the nucleation of semi-coherent precipitates. Consequently, a much more advanced stage of precipitation can exist at the grain boundaries.

Table 1 Activation energy values for β″ precipitation of 6061/10 wt.% SiC composite solutionized at various temperatures

Solution T/ °C	Activation energy/J mol^{-1}		Factor Z
	ASTM	Kissinger	
510	93.500	92.560	$6.52\ 10^{8}$
530	117.943	118.136	$2.48 \cdot 10^{11}$
540	122.308	122.221	$3.37 \cdot 10^{11}$
600	129.706	128.378	$4.28 \cdot 10^{12}$

Another important reason for the increase in activation energy may be the formation of a cluster of Si under the internal stress field. Dutta and Dourell calculated the stress field near SiC fibres by using a finite element method. Since Si forms a substitutional solid solution with Al, the driving force of the stress-assisted diffusion of Si in Al is the relief of hydrostatic stress [9]. Since Si has a smaller atomic radius than that of Al, the Si atoms will diffuse away from regions with tensile hydrostatic stress towards regions with compressive residual hydrostatic stress until an equilibrium condition is reached. Figures 1 and 2 indicate that the heat release for the formation of Si clusters is 1.633 J g^{-1} for the 600°C solutionized specimens, and 0.253 J g^{-1} for the 510°C solutionized specimens. The higher heat flow implies that more heat is released for formation of the Si cluster. In consequence of the relief of internal energy, the MMC becomes more stable, and hence the activation energy is increased.

Thomas and King [14] found that the activation energy E of the MMCs is approximately 21% lower than that of the unreinforced alloys, suggesting that diffusion is easier in MMCs. Nieh and Karlak [22] observed the same trend. They

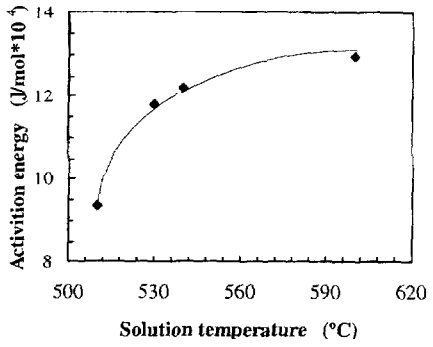

Fig. 3 Activation energies of specimens solution-treated at four different temperatures

attributed the reduction in activation energy for diffusion in the MMC to the enhanced diffusion of solute along dislocations to growing intermediate precipitation. Since MMCs have a larger grain boundary area than that of the unreinforced alloys, solute diffusion is likely to be enhanced due to the fine grain size. Further evidence of reinforcement on precipitation is the shift in the exothermic peaks. It was found that the peak-aging temperature for an Al alloy reinforced with SiC_p or Al_2O_3 could be about 30°C lower than that for the unreinforced Al alloy [23]. Kolobnev *et al.* [24] noted the same trend for 6061 material. This may be attributed to high quench-in dislocations because of the difference in coefficient of thermal expansion between the Al alloy matrix and the SiC particulates. The presence of a high density of vacancies and dislocations allows the occurrence of precipitation at lower temperatures, since diffusion in the substitutional solid-solution is through a vacancy-exchange mechanism. Vacancies play a particularly significant role in the formation of the GP zones [14]. Nucleation of the secondary phase is greatly influenced by the existence of discontinuities in the composite. When the specimen is quenched from high temperature, vacancies, dislocations and locations with great disorder are preferred sites for the nucleation of precipitation. A DSC study on an AA6061 particulate-reinforced MMC led to the conclusion that particulate additions increase the quenching sensitivity, significantly reduce the volume of GP zones formed in the MMC as compared to the monolithic materials, and accelerate the precipitation of intermediate phases [26]. Dutta *et al.* [12] studied the precipitation behaviour of Al_2O_3-reinforced MMCs by means of DSC, TEM and resistivity measurements. They concluded that Al_2O_3 particulates accelerate both the nucleation and the growth of precipitation. The enhancement of nucleation occurs through a reduction of the incubation time for Si clustering, whereas the growth rate is increased due to a higher diffusivity. Both effects are a consequence of the increased density of dislocations due to a thermal expansion coefficient mismatch.

Since the enthalpy ΔH released during precipitation is proportional to the volume fraction of the precipitation according to Eq. (7), the amount of precipitation can be estimated for different solution-treated specimens [1].

$$\Delta H = \frac{\Delta H_p \rho_p}{W_p \rho_s} V_f \tag{7}$$

where ΔH_p is the enthalpy of precipitation, W_p is the molecular weight of the precipitate, ρ_p is the density of the precipitate, ρ_s is the density of the sample and V_f is the volume fraction of precipitation. Therefore, by measuring the change in enthalpy, the extent of precipitation can be determined.

Prediction of precipitation

Two sets of calculated precipitation conversion curves are given in Fig. 4. The conversion calculation is based on Eq. (2) if Z, the pre-exponential factor, and E,

the activation energy, are known. In the case of precipitation, conversion gives the percentages of precipitates during heating. These permit optimal peak-aging temperatures and aging durations to be selected accordingly.

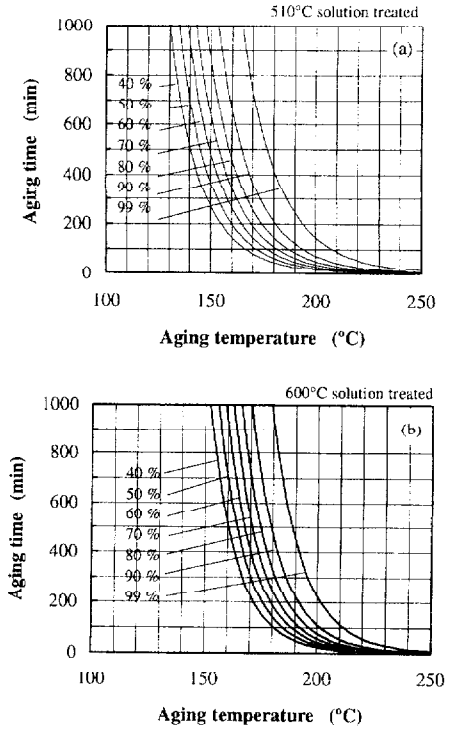

Fig. 4 Conversion curves for determination of aging temperatures and times at solution temperatures of (a) 510 and (b) 530°C

In order to make comparisons between the aging hardness and the conversion curves, microhardness tests were carried out. Figures 5(a) and (b) show the relationships between hardness and aging duration at aging temperatures of 160 and 177°C. The peak-aging times are 480–600 min for the 177°C aging and 900–1000 min for the 160°C aging. Comparison of the peak-aging times with the conversion curve for the 510°C solution treatment in Fig. 4(a) furnishes a peak-aging conversion of about 97% for the specimen aged at 160°C, and of about 95% for that aged at 177°C.

From the measurement of hardness and the precipitation conversion, it was found that the maximum aging hardness can be obtained only when the precipitation conversion is less than 100%. As mentioned before, during aging the GP zones precipitate first and subsequently grow to form the β′ phase. Precipitates of the β′ phase grow with prolonged aging time. The formation of GP zones in-

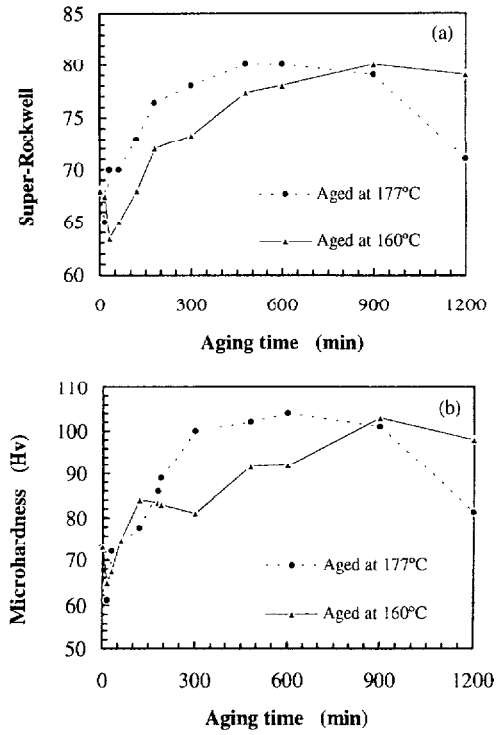

Fig. 5 Relationship between aging time and hardness using (a) microhardness, and (b) super-Rockwell

creases the energy required for the dislocations to break the Mg–Si bonds when they pass through the precipitates, leading to an increase in strength. The strength decreases once the β′ precipitates are formed. However, in the later stage of aging, the growth of GP zones and the formation of β′ precipitates take place at the same time. The decrease in strength due to the dominant effect of the formation of β′ precipitates is manifested in a decrease in hardness.

Conclusions

1. Precipitation in a metal matrix composite can be monitored by using DSC. Three stages of precipitation have been observed in the 6061/10 wt.% SiC_p composite: nucleation and growth of GP zones, and β′ and β phases.

2. The increase in activation energy for the formation of the β″ phase of the solution-treated 6061/10 wt.% SiC_p composite with increase of the solution temperature may be attributed mainly to the phenomenon of grain growth at higher temperatures and the local melting of eutectics. Grain size measurements revealed a grain growth of about 24% when the solution temperature was increased

from 510 to 600°C. The relief of the internal energy due to the formation of Si clusters stabilizes the solutionized metal matrix composite and hence increases the activation energy for GP zone formation.

3. The peak-aging temperature and time can be obtained by using a precipitation conversion curve calculated from DSC thermal curves. In the present study, peak-aging was obtained when about 95 to 97% of the GP zones had been precipitated.

* * *

This project was supported by a grant from the National University of Singapore under RP960653. The authors would also like to thank Prof. M. K. Surappa (I.I.Sc., Bangalore, India) for supplying the composite used in this study.

References

1 D. Richard and P. N. Adler, Metall. Trans., 8A (1977) 1177.
2 P. N. Adler and D. Richard, Metall. Trans., 8A (1977) 1185.
3 J. M. Papazian, R. J. Deiasi and P. N. Adler, Metall. Trans., 11A (1980) 135.
4 J. M. Howe, Aluminium Alloys – their Physical and Mechanical Properties, Vol. 1, ed. E. A. Starke, Jr. and T. H. Sanders, Jr., Intern. Conf. at the Univ. of Virginia, Charlottesville, Virginia, 15–20 June 1986, Pbl. Eng. Mat. Advisory Services Lt., UK, p. 603.
5 C. Badini, F. Marino and E. Verne, Mat. Sci. Eng., 191A (1995) 185.
6 T. Das, S. Bandyopadhyay and S. Blairs, J. Mat. Sci., 29 (1994) 5680.
7 T. G. Nieh and R. F. Karlak, Scripta Metall., 18 (1984) 25.
8 J. W. Cahn, Acta Metall., 5 (1957) 169.
9 I. Dutta and D. L. Bourell, Mat. Sci. Eng., 112A (1989) 67.
10 I. C. Stone and P. Tsakiropoulos, Mat. Sci. Eng., 189 (1994) 285.
11 T. S. Kim, T. H. Kim, K. H. Oh and H. I. Lee, J. Mat. Sci., 27 (1992) 2599.
12 I. Dutta, S. M. Allen and J. L. Hafley, Metall. Trans. A, 22 (1991) 2553.
13 M. Gupta and M. K. Surappa, Key Eng. Mat., 104–107 (1995) 259.
14 M. P. Thomas and J. E. King, J. Mat. Sci., 29 (1994) 5272.
15 Annual Book of ASTM Standards, 14 (1984) 518.
16 H. E. Kissinger, Reaction Kinetics in Differential Thermal Analysis, Anal. Chem., 29 (1957) 1702.
17 S. Suresh, T. Christman and Y. Sufimura, Scripta Metall., 23 (1989) 1599.
18 W. F. Smith, Structure and Properties of Engineering Alloys, McGraw-Hill, Inc., 1993 p. 207.
19 Y. Li and X. An, Rare Metals, 13 (1994) 108.
20 J. M. Papazian, Metall. Trans., 12A (1981) 269.
21 C. Badini, F. Marino and A. Tomasi, J. Mat. Sci., 26 (1991) 6279.
22 T. G. Nieh and R. F. Karlak, Scripta Metall., 25 (1991) 1315.
23 C. Garcia, E. Louis, J. Narciso and A. Pamies, Mat. Sci. Eng., 189A (1994) 219.
24 I. F. Kolobnev, Heat Treatment of Aluminium Alloys, Israel Program for Scientific Translations, Jerusalem 1963.
25 K. R. Van Horn, Aluminium, Vol. 1, American Society for Metals, Metal Park, Ohio, Chapman & Hall, 1967, p. 109.
26 J. M. Papazian, Metall. Trans. A, 19 (1988) 2945.